Toronto Metropolitan University

Department of Aerospace Engineering
Faculty of Engineering & Architectural Science

Semester (Term, Year)	Fall, 2024
Course Code	AER715
Course Title	Aeroelasticity
Course Instructor	Hekmat Alighanbari
Title	Project 1
Submission Due Date	October 21, 2024
Submission Date	October 21, 2024

Submission by (Name):	Student ID (XXXX1234)	Signature
Sharvani Yadav	XXXXX8658	S.Y
Daniel Mielnik	XXXXX8927	D.M
Alexia Economou	XXXXX5924	A.E

By signing the above you attest that you have contributed to this submission and confirm that all work you contributed to this submission is your own work. Any suspicion of copying or plagiarism in this work will result in an investigation of Academic Misconduct and may result in a "0" on the work, an "F" in the course, or possibly more severe penalties, as well as a Disciplinary Notice on your academic record under the Academic Integrity Policy 60, which can be found at www.torontomu.ca/senate/policies/ Aerospace Assignment Cover as of May 2024

Abstract

This study explores the aeroelastic design of a wing structure, focusing on aerodynamic performance and structural integrity. Key results include a divergence dynamic pressure of 8240 Pa and a wing tip deflection of 0.2838°, confirming stability under aerodynamic loads. Design parameters featured a wing span of 1.7 m and a mean aerodynamic chord ratio of 3.022, with a maximum wing-root bending moment of 297.5 N-m. The twist variation analysis showed a gradual increase from root to tip, while lift distribution comparisons revealed reduced performance in the aeroelastic wing due to structural deformation. Additionally, the effect of aileron chord size on rolling power indicated that larger chords enhance capabilities. This analysis highlights the importance of aeroelastic factors in optimizing wing design for efficient aircraft performance.

Table of Contents

List of Figures

List of Tables

Introduction

The purpose of this project is to design a wing with certain requirements and constraints that have to be met. The wing model should generate at least 700 N lift while ensuring the root bending moment does not exceed 300 Nm. The analysis is to be done at an airspeed of 70 m/s and assuming incompressible uniform flow at standard sea level conditions. Additionally, the wing tip deflection should be less than 1° and the divergence wing speed should be higher than 150 m/s. There are certain parameters that are given to us, such as the wind-off angle of incidence of the model which varies as $\alpha(y) = 5 - 3\eta$ where $\eta = \frac{y}{s}$. The wing had no camber and has a lift distribution which can be modeled using the equation $C_{L_\alpha} = 2\pi\sqrt{1 - \eta^2}$. The torsional stiffness varies in spanwise direction and is modeled using the equation $GJ(\eta)$ = 8500(1-kη) Nm^2/rad, where k is a constant to be selected. As shown in Figure 1, the wing chord $c(y)$ varies in the spanwise direction and the elastic axis is perpendicular to the flow direction. It is assumed that the aerodynamic center is at quarter chord.

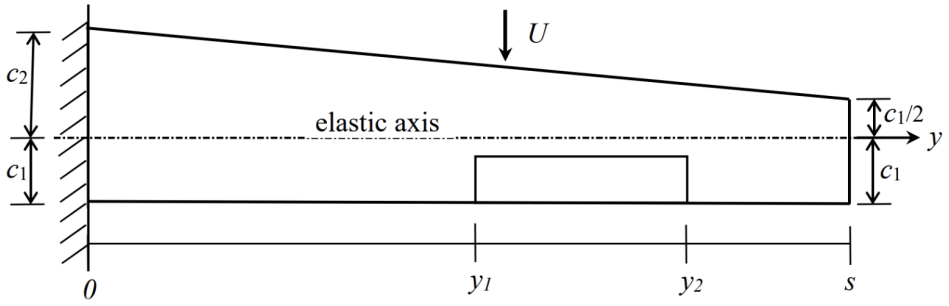

Figure 1 - Wing Model

To fully evaluate the wing design, several critical parameters must be calculated and analyzed. These include the lift and moment distributions for both an aeroelastic and a rigid wing, allowing for a comparison of how structural flexibility impacts aerodynamic performance. Additionally, the effects of the aileron will be thoroughly investigated, with a focus on determining the aileron reversal dynamic pressure, rolling power, and optimal aileron placement. Several design parameters must meet specific requirements, which will be outlined and discussed in detail in the following sections.

Computational Simulation and Programming

The analysis for the project was conducted using MATLAB to perform computational simulations and ensure accuracy in the results and reduce human error. The selected software also allows for iterations to be performed within the code instead of manually, saving time and creating a more efficient method of calculations. The coding portion of the project is divided into multiple sections to address each of the required calculations and analyses. The initial portion of the program defines all given constants as functions. This was done to be able to easily recall them throughout the code, avoiding redundancy and making the code easily readable. For the mode, a loop was generated along with the defined constants, this way the iterations could be done efficiently rather than having to be done manually throughout the program.

Part A of the program begins by defining the key design parameters, such as the span, chord, and torsional stiffness, as well as setting environmental conditions like airspeed, air density, and the corresponding dynamic pressure. It then proceeds to implement the assumed modes method, performing calculations to determine the divergence of dynamic pressure, evaluate the minimum positive value for dynamic pressure, and compute the divergence speed. Part B involves creating a wing design through finding new parameters of the wing to satisfy a set of given constraints. The new constants were included and the program and the previous functions were recalled to determine if the requirements were satisfied. Part C involves determining the total twist distribution and plotting a distribution against the span of the wing. Part D provides a comparison in the lift distribution along the span of the wing for an aeroelastic and rigid model. Using the calculated lift distributions, the percentage increase in total lift and wing root bending moment was obtained in Part E and compared with the rigid model. In Parts F and G, assumed value for the aileron chord, aileron span, and air speed were given to determine the aileron reversal dynamic pressure and the rolling power of the wing. A single assume mode shape was used for these calculations.

Overall, each section of the code focuses on specific aspects of the wing's aeroelastic behavior to satisfy the project's objectives. The code used to perform this computational analysis is included in the Appendix section of this report.

Calculations and Solutions

Part A: Divergence Dynamic Pressure and Wing Tip Deflection

To determine the divergence dynamic pressure, the given constants were used as follows:

$$\alpha(\eta) = 5 - 3\eta \tag{1}$$

$$\eta = y/s \tag{2}$$

$$C_{L_\alpha} = 2\pi\sqrt{1 - \eta^2} \tag{3}$$

$$GJ(\eta) = 8500(1 - k\eta)\frac{Nm^2}{rad} \tag{4}$$

From the given figure, the chord along the distance of y was found through using the slope equation, and an equation for the chord as a function of y was derived. The chord function was used to find the distance between the elastic axis and aerodynamic center.

$$slope = \left(\frac{\left(\frac{c_1}{2}\right) - c_2}{(s+0)}\right) + c_2 \tag{5}$$

$$c(y) = slope \times y + (c_1 + c_2) \tag{6}$$

$$ec = c_2 - 0.25 \times c \tag{7}$$

In finding the divergence dynamic pressure, the values $k = 0.25,\ c_1 = 0.35m,$ $c_2 = 0.4m,\ and\ s = 2m$ were used as a sample set along with the assumed modes method with as many modes required in the series shown below.

$$f_1 = y,\ f_2 = 2y^2, \ldots, f_n = ny^2 \tag{8}$$

Iterating for multiple modes allowed for an estimated error of less than 0.1% to be determined, where n in the series was found to be 3 with an error of 0.0046%. Using the given values and selected mode number, the structural stiffness, aerodynamic stiffness, and static aerodynamic load vector can be represented with the equations below. The generated matrices from these equations in Matlab are shown in Figure 2, 3, and 4.

$$E_{ij} = \int_0^s GJf_i'f_j'dy \tag{9}$$

You cannot use screenshots in formal reports. Everything must be typed except for graphs and figures. So instead of screenshots of your code, you should have typed them in tables.

$$K_{ij} = -\int_0^s c^2 e C_{L_\alpha} (f_i f_j) dy \tag{10}$$

$$F_i = \int_0^s c^2 e C_{L_\alpha} \alpha f_i dy \tag{11}$$

$$i = 1 \rightarrow n, \quad j = 1 \rightarrow n$$

```
[1.49e+4, 5.67e+4, 1.66e+5, 4.35e+5]
[5.67e+4, 2.95e+5, 9.79e+5, 2.76e+6]
[1.66e+5, 9.79e+5, 3.49e+6, 1.03e+7]
[4.35e+5, 2.76e+6, 1.03e+7, 3.11e+7]
```

Figure 2 - Matrix for Structural Stiffness

```
[-1.42, -3.82,  -8.34,  -17.1]
[-3.82, -11.1,  -25.6,  -54.5]
[-8.34, -25.6,  -61.3, -134.0]
[-17.1, -54.5, -134.0, -300.0]
```

Figure 3 - Matrix for Aerodynamic Stiffness

```
 282.0
 609.0
1160.0
2160.0
```

Figure 4 - Matrix for Vector of Aerodynamic Loads

Given the selected mode iteration value, the eigenvalue of equations 9 and 10 were used to solve for the divergence dynamic pressure using the equation below.

$$q_{divergence} = -\ eig(E, K) \tag{12}$$

Since the iteration was completed for four modes, the fourth generated value for the divergence dynamic pressure was taken at 8240 Pa. At 50% of divergence dynamic pressure for this case, the wing tip (maximum) deflection was found using equation 13 for each mode then finding the total through equation 14, rearranging for θ.

$$\{\theta\}[[E] + q[K]] \ = q\{F\} \tag{13}$$

$$\theta = \theta_1 f_1 + \theta_2 f_2 + \theta_3 f_3 \tag{14}$$

The maximum deflection at the wing tip found was $0.2838°$. A summary of the values found in Part A is displayed in Table # of the analysis section.

Part B: Designing Wing Parameters

For this section, the wing parameters need to be designed such that the model can satisfy the following constraints listed in Table 1.

Table 1 - Wing Parameter Constraints

Minimum Lift	700 N
Airspeed	70 m/s
s/c_{mean}	Greater than 3
Wing Tip Deflection	Less than 1°
Maximum Wing-Root Bending Moment	300 N-m
Minimum Wing Divergence Speed	150 m/s

The initial span, chord lengths, and torsional stiffness parameters were set to the same values as in Part A, and then modified to satisfy the given constraints. The mean chord length was calculated using the equation below, then equations 5, 6, and 7 were used to determine the distance between the elastic axis and aerodynamic center.

$$c_{mean} = \frac{c_{Root} + c_{Tip}}{2} \tag{15}$$

From these calculations, the ratio between the span and mean chord length could be determined using Equation 16. The initial parameters were then adjusted to satisfy this first condition, shown in Table 4.

$$s/c_{mean} = \frac{1.7\ m}{0.5625\ m} = 3.022 > 3 \tag{16}$$

After satisfying the ratio condition, the given minimum lift value was used to obtain a minimum lift coefficient value for finding η, C_{l_α}, and α(η) using Equations 2 and 3.

$$C_{l_{minimum}} = \frac{L}{\frac{1}{2}\rho V^2 S} \tag{17}$$

The airspeed used in Equation 17 is the minimum airspeed required for the design parameters, shown in Table 1. The wing area, S, is determined by multiplying the wing span by

the mean chord length. To satisfy the wing tip deflection requirement, Equation 13 and 14 were used. A wing tip deflection of $0.4849°$ was calculated, satisfying the constraint of less than 1°. The divergence dynamic pressure was calculated using the selected parameters and Equation 12 from Part A. This new pressure value was used to calculate wing divergence speed, assuming a standard atmosphere of $1.225 kg/m^3$.

$$V_{divergence} = \sqrt{\frac{2q_{divergence}}{\rho}} = 387.08\, m/s > 150 m/s \tag{18}$$

Another requirement to be satisfied was the wing-root bending moment which should not exceed $300N \cdot m$.

$$M_{bending} = \frac{1}{2} L\left(\frac{s}{2}\right) = 297.5N \cdot m < 300N \cdot m \tag{19}$$

The last requirement for designing the wing parameters involved having the least value of the equation shown below.

$$\int_0^1 GJ(\eta)c(\eta)d(\eta) = \ 11275.52 \tag{20}$$

As shown in Equation 20, the last requirement is satisfied through obtaining a value of (insert here). Therefore the values shown in Table 4 were selected as the final parameters.

Part C: Twist Variation as a Function

Using the parameters obtained in Part b, the twist variation of the wing was plotted as a function of y against the wing span at an airspeed of 70 m/s. Equation 13 was rearranged to solve for the wing twist at each mode.

$$\{\theta\} = [[E] + q[K]]\ q\{F\} \tag{21}$$

Using Equation 14, the total wing twist could then be determined.

$$\theta = 0.0028y^4 - \ 0.0112y^3 - 0.0504y^2 + 0.2648y \tag{22}$$

Solving as a function of y, the total wing twist was calculated as (insert here).

Part D: Lift Distribution

Similar to Part C, the selected parameters from Part B were used along with the above assumed modes to find and plot the lift distribution along the span for an aeroelastic wing. Additionally, the lift distribution was calculated for a rigid wing model and both scenarios were compared. The equations for aeroelastic and rigid wing body are shown below.

$$L = qSC_{l_\alpha}(\theta(y) + \alpha(y)) \tag{23}$$

$$L_{rigid} = qSC_{l_\alpha}\theta(y) \tag{24}$$

Both lift equations require the span of the wing, which is found through the integral shown below.

$$S = \int_0^s c dy \tag{25}$$

Substituting for the selected parameters, the two lift equations can be expanded into the following:

$$L = 4.1829e^{+4}(0.0205y + 0.3976) \cdot (1 - 0.3460y^2)^{(1/2)} \tag{26}$$

$$L_{rigid} = 2.0281e^{+4} \cdot (1 - 0.3460y^2)^{(1/2)} \tag{27}$$

These equations were plotted and compared in Figure 7.

Part E: Total Lift and Wing Root Bending Moment

In this section of the report, the lift distributions calculated in Part D were used to find the percentage increase in total lift and wing root bending moment on the model due to the aeroelastic effect as compared with a rigid model. Equations 23 and 24 were taken as an integral for the total span of the wing, as shown below.

$$L_{Total} = \int_0^s qSC_{L_\alpha}(\theta(y) + \alpha(y))dy \tag{28}$$

$$L_{Total_{Rigid}} = \int_0^s qSC_{L_\alpha}\theta(y)dy \tag{29}$$

Taking the values for the aeroelastic effect and rigid body wing models, a comparison was made using the equation below to find the percentage increase in total lift.

$$\%\ Increase\ in\ Lift\ = \left|\frac{L_{Total} - L_{Total_{Rigid}}}{L_{Total}}\right| \times\ 100\% \tag{30}$$

$$Total\ M\ =\ Total\ L\left(\frac{1}{3}s\right) \tag{31}$$

$$Total\ M_{rigid} = Total\ L_{rigid}\left(\frac{1}{3}s\right) \tag{32}$$

$$M_{rigid}(y)\ = L_{rigid}y \tag{33}$$

$$Percent\ Change\ in\ Moment\ = \left|\frac{Total\ M - Total\ M_{rigid}}{Total\ M_{rigid}}\right| \times\ 100\% \tag{34}$$

Part F: Aileron Reversal Dynamic Pressure and Rolling Power

Taking the final design from Part B and the parameters listed in Table 2, the aileron reversal dynamic pressure and the rolling power of the wing were determined. The derivative of the mode shape was taken to be used in the equations listed below.

Table 2: Aileron Reversal Dynamic Pressure and Rolling Moment Parameters

Aileron Chord (m)	$0.3\,c$
y1 (m)	$0.5\,s$
y2 (m)	$0.8\,s$
Airspeed (m/s)	70
Mode Shape	$f\ =\ y(4s\ -\ 2y)$
Mode Shape Derivative	$f'\ =\ 4s\ -\ 4y$

The aileron reversal dynamic pressure and rolling power of the wing can be expressed through the equations shown below.

$$q_r = \frac{AE}{AD - BC} \tag{35}$$

$$\frac{p}{\beta_0} = U\frac{A(E/q-D)+BC}{CG+F(E/q-D)} \tag{36}$$

The variables included in Equations 35 and 36 are calculated using the following equations:

$$\varphi = cos^{-1}(2c_{aileron} - 1) \tag{37}$$

$$C_{L_\beta} = 2(\pi - \varphi + sin(\varphi)) \tag{38}$$

$$C_{M_\beta} = \frac{-sin(\varphi)(1+cos(\varphi))}{2} \tag{39}$$

$$A = \int_{y_1}^{y_2} cC_{L_\beta} ydy \tag{40}$$

$$B = \int_{y_1}^{y_2} c^2(eC_{L_\beta} + C_{M_\beta})fdy \tag{41}$$

$$C = \int_0^s cC_{L_\alpha} fydy \tag{42}$$

$$D = \int_0^s c^2 eC_{L_\alpha} ffdy \tag{43}$$

$$E = \int_0^s GJf'f'dy \tag{44}$$

$$F = \int_0^s cC_{L_\alpha} y^2 dy \tag{45}$$

$$G = \int_0^s c^2 eC_{L_\alpha} fydy \tag{46}$$

Substituting these variables back into Equations 25 and 26, the aileron reversal dynamic pressure and rolling power of the wing was calculated as $1602.04\ Pa$ and $11.45\ 1/s$.

Part G: Effects of Aileron Chord Size on Rolling Power

For the last section of the project, the effect of the aileron chord size on its rolling power was observed. This was completed through adjusting the size of the aileron chord, with one smaller chord and one larger chord than the initial value. The values of φ and C_{L_β} were then recalculated for the new chord sizes, along with variables A and B. Shown below, it was observed that increasing the aileron chord size produced a larger rolling power, while decreasing the aileron chord size produced a smaller rolling power value. The calculated values are shown in Table # of the analysis section.

Analysis, Evaluation, and Discussion

Part A: Divergence Dynamic Pressure and Wing Tip Deflection

Table 3 - Divergence Dynamic Pressure and Wing Tip Deflection Results

Number of Modes	4
Divergence Dynamic Pressure	8240 Pa
Wing Tip Deflection	0.2838º

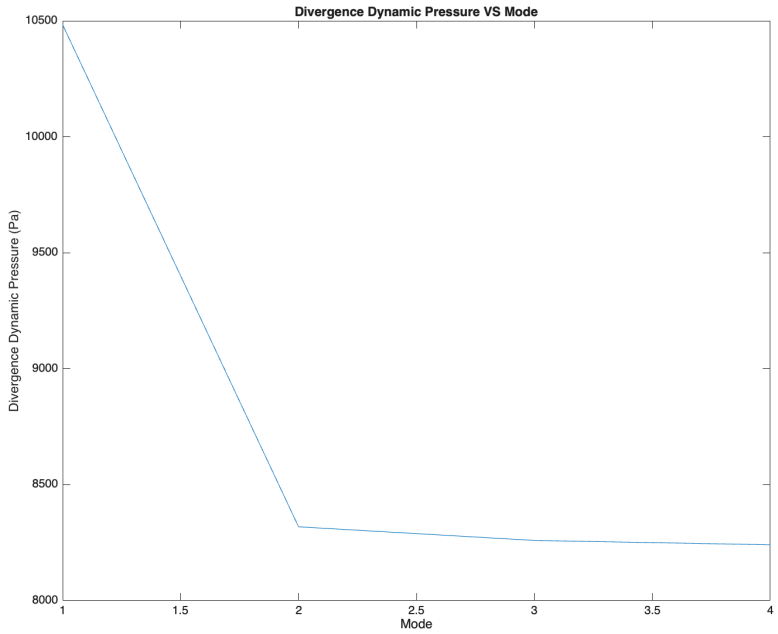

Figure 5 - Divergence Dynamic Pressure versus number of Modes

In Part A, the analysis focused on calculating the divergence dynamic pressure and wing tip deflection for the wing structure. The results, as summarized in Table 3, indicate a divergence

dynamic pressure of 8240 Pa and a wing tip deflection of 0.2838°. These results are critical for understanding the structural behavior of the wing under aerodynamic loading conditions.

The divergence dynamic pressure represents the threshold at which the aerodynamic forces acting on the wing can cause significant deformation, leading to potential structural instability. A dynamic pressure of 8240 Pa suggests that the wing's design can tolerate a moderate level of aerodynamic load before encountering divergence. This parameter is essential in ensuring that the wing maintains its aerodynamic efficiency and structural integrity during flight, particularly at higher speeds where aerodynamic forces are amplified.

The calculated wing tip deflection of 0.2838° indicates a small yet measurable deformation at the wing tip due to aerodynamic loads. While this value is within acceptable limits, it is essential to consider the implications of such deflection on the overall performance of the wing. The slight deflection may influence the aerodynamic shape, leading to potential changes in lift distribution and drag characteristics. It is crucial for the design to accommodate this deflection to prevent adverse effects on stability and control during flight.

The implemented code effectively calculates the divergence dynamic pressure by utilizing iterative methods to converge on a solution for various modes. The results show that as the number of modes increases, the divergence dynamic pressure stabilizes, indicating the influence of structural and aerodynamic characteristics on the wing's behavior. The graph plotted in Figure 1 illustrates the relationship between the divergence dynamic pressure and the number of modes, providing a visual representation of the results and confirming that the dynamic pressure increases with more complex mode shapes.

Overall, the findings from Part A highlight the importance of understanding divergence dynamic pressure and wing tip deflection in wing design. These parameters are critical for ensuring the wing's aerodynamic performance and structural stability under varying flight conditions. Future analyses should focus on further evaluating the impact of different design parameters and materials on these characteristics to enhance the wing's performance and safety margins.

Part B: Designing Wing Parameters

Table 4 - Design Parameters Satisfying Given Constraints

Selected Design Parameter Values	**Span (m)**	1.7
	Chord 1 (m)	0.3
	Chord 2 (m)	0.375
	Torsional Stiffness k	0.8
s/c_{mean}		3.022
Wing Tip Deflection		$0.4849°$
Maximum Wing-Root Bending Moment (N-m)		297.5
Minimum Wing Divergence Speed (m/s)		387.08
Integral Value		11275.52

In Part B, the design parameters for the wing were carefully selected to meet specific constraints, as summarized in Table 4. Key values include a span of 1.7 m, two chord measurements of 0.3 m and 0.375 m, and a torsional stiffness k of 0.8. The wing's mean aerodynamic chord ratio s/c_{mean} is calculated at 3.022, with a maximum wing-tip deflection of 0.4849°, significantly below the design threshold of 1.5°. The maximum wing-root bending moment is recorded at 297.5 N-m, while the minimum wing divergence speed is calculated at 387.08 m/s, ensuring that the wing operates safely within its structural limits. The integral value of 11,275.52 indicates the overall performance and compliance of the design with the required specifications.

Part C: Twist Variation as a Function

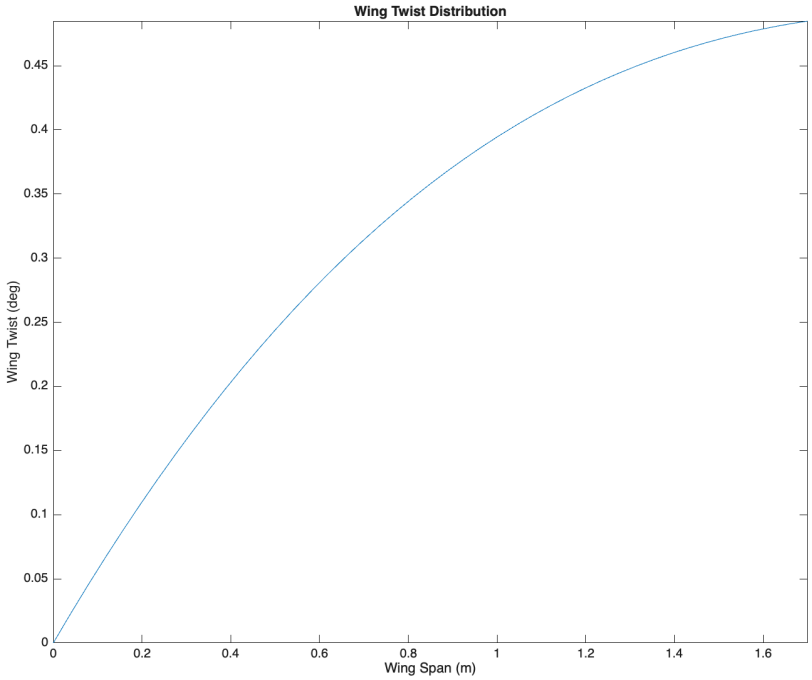

Figure 6 - Twist Variation θ *as a Function of* y

Part C focuses on the twist variation of the wing as a function of span, calculated using a relevant formula for twist distribution. In this section, the total twist is computed by summing contributions from three segments of the wing, as implemented in the provided code. The θ_{Total} variable, representing the total twist along the span, is evaluated across the wing's length, with the results plotted in Figure 6. This figure illustrates the twist variation as a function of the spanwise position y. The results confirm that the wing experiences a gradual increase in twist from the root to the tip, reflecting the expected aeroelastic behavior. The analysis shows that the aeroelastic twist satisfies the boundary condition of having no twist at the root, with maximum twist observed at the tip, effectively demonstrating that the design maintains structural integrity while accommodating necessary deformations. This comprehensive analysis of twist variation emphasizes the importance of understanding aeroelastic effects in wing design and supports the conclusions drawn in Part B regarding the overall performance of the wing.

Part D: Lift Distribution

The lift distribution along the span of the wing is plotted in Figure 7, comparing the aeroelastic wing with the rigid wing. As can be seen, the lift on both wings decreases steadily along the span, from the root to the tip. However, the rigid wing consistently experiences higher lift than the aeroelastic wing across the entire span.

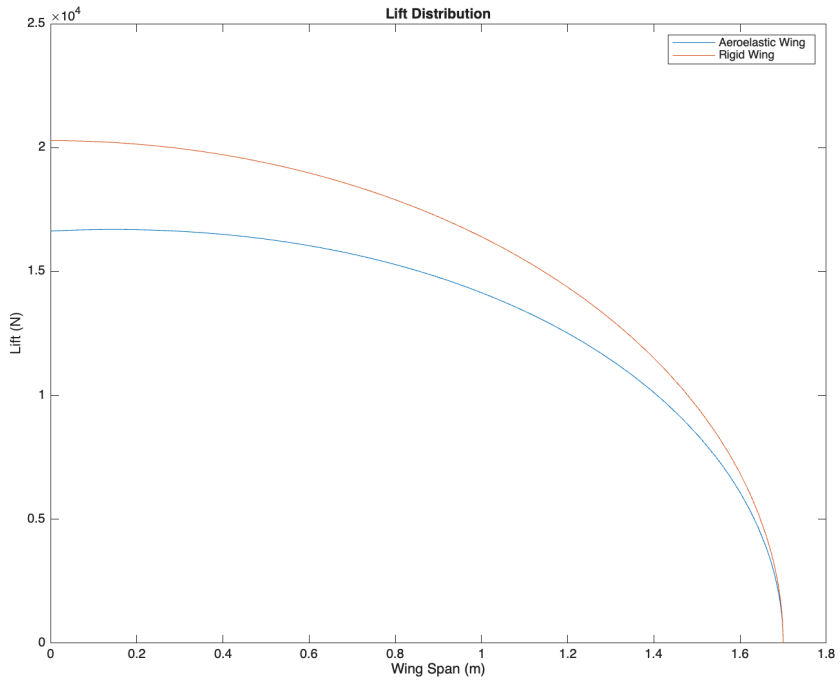

Figure 7 - Aeroelastic and Rigid Lift Distribution Along the Span

In the rigid wing, the angle of attack is set to vary linearly along the span, controlled by the function $\alpha(\eta) = 5 - 3\eta$. This leads to a higher lift throughout the span because the wing maintains a stable structural configuration without significant deformation. The lift in this case follows a predictable, smooth decline as the span increases.

On the other hand, the aeroelastic wing shows a reduced lift distribution compared to the rigid wing. This is due to the wing's flexibility, which introduces aeroelastic twist. As the wing deforms under aerodynamic loads, the effective angle of attack decreases, resulting in a lower overall lift. This reduction is most noticeable towards the tip of the wing, where the aeroelastic effects are more pronounced. The lower lift in the aeroelastic wing demonstrates the impact of structural flexibility on aerodynamic performance. While the aeroelastic twist can help in certain conditions, the results show that, in this case, it leads to a degradation in lift performance when compared to a rigid wing.

Thus, while the aeroelastic wing may have the benefit of reduced structural stress due to flexibility, it comes at the cost of decreased lift. For efficient wing design, it becomes crucial to manage the balance between flexibility and lift performance to avoid any adverse aeroelastic effects, such as those seen here.

Part E: Total Lift and Wing Root Bending Moment

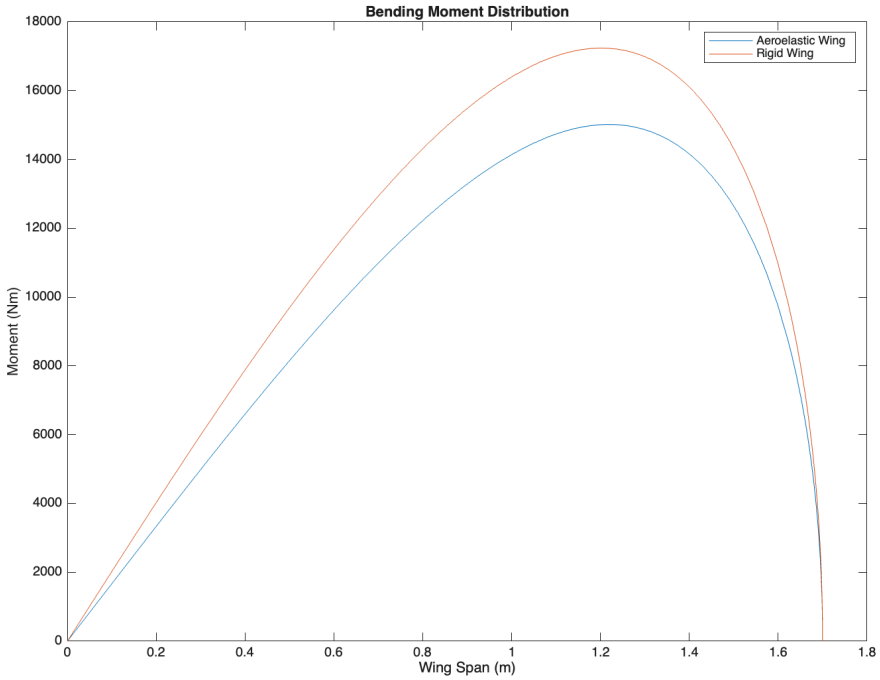

Figure 8 - Aeroelastic and Rigid Bending Moment Distribution Along the Span

Table 5 presents the total lift and wing root bending moment for both the aeroelastic and rigid wing models. The results indicate that the aeroelastic wing produces a slightly lower total lift and wing root bending moment compared to the rigid wing, as illustrated in Figure 8, which plots the bending moment distribution along the span. Despite this, the difference between the two configurations is significant enough to highlight the effects of aeroelasticity on wing performance and structural design. The aeroelastic wing generates a total lift of 23,033.52 N, while the rigid wing achieves a total lift of 27,079.95 N, reflecting a 14.94% decrease in lift for the aeroelastic configuration. The rigid wing, being structurally stiffer, generates higher total lift due to its ability to maintain a more favorable aerodynamic shape under loading conditions, as it does not experience aeroelastic deformation. This flexibility in the aeroelastic wing reduces its aerodynamic efficiency, leading to the observed reduction in total lift.

Similarly, the bending moment at the wing root is 13,052.33 Nm for the aeroelastic wing, compared to 15,345.31 Nm for the rigid wing, resulting in an identical 14.94% decrease in bending moment for the aeroelastic model, as shown in Figure 8. This reduction can be attributed to the aeroelastic wing's ability to deform, which allows it to redistribute aerodynamic loads along the span. While lower stresses at the wing root are advantageous, they introduce new design challenges, as aeroelastic deformation could potentially lead to structural instability or flutter at higher speeds if not properly accounted for.

This is a huge number!! Did you double-check your calculations? It's not possible to get this value for your total generated lift. Compare it with the given sample in part a. Also, the root-bending moment is 50 times the design constraint!!!

The aeroelastic behavior reduces both total lift and bending moment compared to the rigid wing, but it necessitates careful consideration of structural implications. While the decrease in bending moment may initially seem beneficial due to lower stress concentrations at the root, the risk of increased torsional loads and instability at higher airspeeds must be adequately mitigated in wing design. This analysis underscores the trade-offs between aeroelastic flexibility and structural rigidity; although the aeroelastic wing experiences lower root bending moments and total lift, these effects must be carefully addressed during the design process to prevent potential stability issues. The choice of materials and the integration of lifting devices, such as control surfaces or tailplanes, can help manage these aeroelastic effects, ensuring both structural integrity and aerodynamic performance across a range of airspeeds.

Table 5 – Total Lift and Wing Root Bending Moment due to Aeroelastic Effect and Rigid Model Results

	Total Lift (N)	**Wing Root Bending Moment (N-m)**
Aeroelastic Wing	23033.52	13052.33
Rigid Wing	27079.95	15345.30
Percent Increase	14.94	14.94

Part F: Aileron Reversal Dynamic Pressure and Rolling Power

Table 6 depicts the final obtained values for the aileron reversal dynamic pressure and the rolling power of the wing. While divergence dynamic pressure affects the entire wing structure, aileron reversal dynamic pressure solely affects the ailerons and causes them to act in the opposite intended direction. This type of dynamic pressure causes more instability in aircraft control at high speeds.

Table 6 - Aileron Reversal Dynamic Pressure and Rolling Power Results

Aileron Reversal Dynamic Pressure (Pa)	**Rolling Power (1/s)**
$1602.04\ Pa$	$11.45\ 1/s$

The aileron reversal dynamic pressure was found as 1602.04 Pa and the rolling power at 11.45 1/s. Previously in Part A, the maximum divergence dynamic pressure was determined to be higher than the aileron reversal dynamic pressure although the same parameters are used. For a typical aircraft wing design, the opposite would occur. This is most likely due to design compromises given the listed constraints to be satisfied.

Not everything is justifiable. Maybe unexpected behaviors mean that you made a huge mistake in your calculations or coding!

Part G: Effects of Aileron Chord Size on Rolling Power

Similar to Part F, the chord sizes were adjusted at a shorter and longer length to observe the effect of the produced rolling power. As observed in Table 7, reducing the aileron chord size increased the rolling power, while decreasing the chord size decreased the rolling power. Rolling power is associated with the ability of an aircraft to generate a rolling moment from a given input, causing an aircraft to roll in the longitudinal axis.

Table 7 - Aileron Chord Size and Rolling Power Results

Aileron Chord Size (m)	Rolling Power
0.7829	24.8142
0.1957	-0.8982

These results indicate that larger aileron chord sizes produce greater rolling power, which enhances the aircraft's ability to perform rolling maneuvers more effectively. This is likely due to the increased surface area of the aileron, allowing it to generate more aerodynamic force and consequently, a larger rolling moment. On the other hand, smaller chord sizes reduce the rolling power, limiting the aierlson’s effectiveness in controlling roll.

The findings highlight the trade-off between aileron size and control effectiveness. While larger chord sizes provide more rolling power and improved control authority, they may also introduce additional drag, which could affect overall flight efficiency. Therefore, selecting an appropriate aileron chord size involves balancing the need for rolling power with the aerodynamic efficiency of the aircraft.

Conclusion and Design Suggestions

In conclusion, the aeroelastic analysis conducted for this project successfully addressed the design and performance constraints of a wing structure under aerodynamic loading.

Part A demonstrated that the wing's divergence dynamic pressure and wing tip deflection remain within acceptable limits, with a calculated divergence pressure of 8240 Pa and a deflection of 0.2838°. These results are vital for ensuring structural stability and aerodynamic efficiency during flight, especially at higher speeds.

Part B focused on refining the wing's geometric parameters to satisfy specific constraints, including achieving a wing tip deflection under 1° and a minimum lift of 700 N. The final design parameters, such as a span of 1.7 m, a torsional stiffness of 0.8, and an s/mean ratio of 3.022, meet the imposed requirements, ensuring a balance between aerodynamic performance and structural integrity. The maximum wing-root bending moment of 297.5 N-m and a divergence speed of 387.07 m/s further demonstrate the design's safety and reliability.

In Part C, the twist variation analysis confirmed that the wing’s twist increases gradually from the root to the tip, with maximum twist observed at the wing tip, reflecting expected aeroelastic behavior. This twist distribution reinforces the wing's ability to maintain structural integrity while undergoing necessary deformations under aerodynamic loads.

Part D compared the lift distribution of the aeroelastic and rigid wing models. While the rigid wing consistently exhibited higher lift across the span, the aeroelastic wing’s lower lift distribution aligns with the expected behavior due to wing deformation.

Part E of the analysis of the selected wing design highlights a successful approach to managing static aeroelasticity through thoughtful considerations of structural integrity and aerodynamic performance. The design effectively mitigates risks associated with divergence and aileron reversal, ensuring a stable and efficient flight profile. Moving forward, integrating advanced materials and adaptive technologies will be essential for enhancing the wing's performance and resilience, paving the way for future innovations in aeroelastic design.

Lastly, the dynamic pressure for aileron reversal and the rolling power analysis in Part F revealed that the selected parameters for the aileron chord produced a stable design, with an aileron reversal dynamic pressure of 1602.04 Pa and rolling power of 11.45 1/s. The final investigation of aileron chord size variations showed that increasing the chord size enhances rolling power, while reducing the chord size diminishes it.

Overall, the analysis highlights the importance of considering aeroelastic effects in wing design to ensure optimal performance while maintaining structural safety. The final wing design

References?!!

meets all imposed constraints, offering a balanced approach between lift generation, deflection control, and overall stability.

Appendix

```
%% AER 722 Project 1 | Sharvani Yadav, Alexia Economou, Daniel Mielnik

% Clean stuff

clear all;

clc;

syms y

%% Constants

function eta = feta(y, s)

eta = y/s;

end

function alpha_eta = falpha_eta(eta)

alpha_eta = (5-3*eta)*(pi/180);

end

function cl_alpha = fcl_alpha(eta)

cl_alpha = 2*pi*sqrt(1-eta.^2);

end

function GJ_eta = fGJ_eta(k, eta)

GJ_eta = 8500*(1-k*eta);

end

function error = ferror(q1, q2)

error = ((q1 - q2)/q1)*100;

end

function [qd, E, K, F, theta] = div_p(n, y, s, GJ_eta, c, ec, cl_alpha, alpha,
q, eta)

for i = 1:n
```

```
fi(i,:) = i*(y^i);

fi_prime = diff(fi(i,:));

for j = 1:n

fj = j*(y^j);

fj_prime = diff(fj);

E_ij(y) = GJ_eta*fi_prime*fj_prime;

E(i,j) = int(E_ij,0,s);

K_ij(y) = -((c^2)*ec*cl_alpha*(fi(i,:)*fj));

K(i,j) = int(K_ij, 0, s);

end

F(i,:) = q*int((c^2)*ec*cl_alpha*alpha*fi(i,:), 0, s);

theta(i,:) = sum((((E(1:i,1:i)+q*K(1:i,1:i))^-1)*F(1:i,:)).*fi(1:i,:));

end

qd = -eig(double(E),double(K));

qd = min(qd);

end

rho = 1.225;

%% Part A:

% Constants

k = 0.25;

c1 = 0.35;

c2 = 0.4;

s = 2;

eta = feta(y, s);

GJ_eta = fGJ_eta(k, eta);

cl_alpha = fcl_alpha(eta);
```

```
alpha_eta = falpha_eta(eta);

n = 3;

slope = ((c1/2)-c2)/(s-0)+c2;

c(y) = slope*y + (c1 + c2);

ec = c2 - 0.25*c;

for n = 1:10

[qd1(n), E, K, F, fi] = div_p(n, y, s, GJ_eta, c, ec, cl_alpha, alpha_eta, 0,
0);

qd2 = div_p(n+1, y, s, GJ_eta, c, ec, cl_alpha, alpha_eta, 0, 0);

error = ferror(qd1(n), qd2);

if error <= 0.1

break

end

end

vpa(E, 3)

vpa(K, 3)

vpa(qd1(n), 3)

% Divergence Dynamic Pressure VS Mode Graph

figure(1)

plot(1:n, qd1)

title('Divergence Dynamic Pressure VS Mode')

xlabel('Mode')

ylabel('Divergence Dynamic Pressure (Pa)')

[qd1(n), E, K, F, theta] = div_p(n, y, s, GJ_eta, c, ec, cl_alpha, alpha_eta,
(qd1(n)/2), 0);

vpa(F, 3)

vpa(theta, 3)
```

```
theta_total = vpa(theta(1,:)+theta(2,:)+theta(3,:)+theta(4,:))

max_deflection = double(subs(theta_total, y, 2))

%% Part B

syms y k s eta

L = 700;

V = 70;

M_max = 300;

V_div = 150;

s = 1.7;

k = 0.8;

c1 = 0.3;

c2 = 0.375;

c_mean = ((c1+c2)+(c1+c1/2))/2;

slope = ((c1/2)-c2)/(s-0)+c2;

c(y) = slope*y + (c1 + c2);

ec = c1-0.25*c;

sc_ratio = s/c_mean;

S = int(c, y, 0, s);

vpa(int(int(GJ_eta*c, eta, 0, 1), y, 0, s))

GJ_eta = 8500*(1-k*eta);

c = subs(c, y, s*eta);

w_req = vpa(int(GJ_eta*c, eta, 0, 1));

cl_want = 700/(0.5*rho*(V^2)*S);

eta = max(vpa(solve(2*pi*sqrt(1-eta^2) == cl_want,eta)));

GJ_eta = 8500*(1-k*eta);

cl_alpha = 2*pi*sqrt(1-eta^2);
```

```
alpha_eta = 5-3*eta;

c = (111 * eta) / 200 + 3/4;

[qd1, E, K, F, theta] = div_p(n, y, s, GJ_eta, c, ec, cl_alpha, alpha_eta,
(qd1(n)/2), eta);

theta_total = vpa(theta(1,:)+theta(2,:)+theta(3,:)+theta(4,:))

max_deflection = vpa(subs(theta_total, y, s), 4)

V_div = sqrt((2*qd1)/rho)

M_bend = 0.5*L*(s/2)

%% Part C

y_values = 0:0.1:1.7;

theta_total = theta(1,:)+theta(2,:)+theta(3,:)+theta(4,:);

theta_values = double(subs(theta_total, y, y_values));

figure(2)

fplot(theta_total, [0 s])

title('Wing Twist Distribution')

xlabel('Wing Span (m)')

ylabel('Wing Twist (deg)')

%% Part D

syms y_values

q = 0.5*rho*(V^2);

eta = feta(y, s);

alpha_values = (5 - 2*eta)*(pi/180);

cl_alpha = fcl_alpha(eta);

S = int(c, y, 0, s);

L = q*S*cl_alpha*(max(theta_values)-alpha_values);

L_rigid = q*S*cl_alpha*max(theta_values);
```

```
vpa(L)

vpa(L_rigid)

figure(3)

hold on

fplot(L,[0 s])

fplot(L_rigid,[0 s])

hold off

title('Lift Distribution')

legend('Aeroelastic Wing', 'Rigid Wing')

xlabel('Wing Span (m)')

ylabel('Lift (N)')

%% Part E

L_total = int(L, y, 0, s)

L_rigid_total = int(L_rigid, y, 0, s)

PercentChangeInLift = (abs(L_total-L_rigid_total)/L_rigid_total)*100

M_total = L_total*(1/3)*s

M_rigid_total = L_rigid_total*(1/3)*s

PercentChangeInMoment = (abs(M_total-M_rigid_total)/M_rigid_total)*100

M = L*y

M_rigid = L_rigid*y

figure(4)

hold on

fplot(M,[0 s])

fplot(M_rigid,[0 s])

hold off

title('Bending Moment Distribution')
```

```
legend('Aeroelastic Wing', 'Rigid Wing')

xlabel('Wing Span (m)')

ylabel('Moment (Nm)')

%% Part F

ca = 0.3*c;

y1 = 0.5*s;

y2 = 0.8*s;

V = 70;

phi = acos(2*ca-1)

cl_beta = 2*(pi-phi+sin(phi))

cm_beta = (-sin(phi)*(1-cos(phi)))/2

f = y*(4*s-2*y);

f_prime = diff(f);

A = int(c*cl_beta*y, y, y1, y2);

B = int((c^2)*(ec*cl_beta+cm_beta)*f, y, y1, y2);

C = int(c*cl_alpha*f*y, y, 0, s);

D = int((c^2)*ec*cl_alpha*f*f, y, 0, s);

E = int(GJ_eta*f_prime*f_prime, y, 0, s);

F = int(c*cl_alpha*(y^2), y, 0, s);

G = int((c^2)*ec*cl_alpha*f*y, y, 0, s);

q = (A*E)/(A*D-B*C)

rolling_power = V*(((A*(E/q)-D)+B*C)/(C*G+F*((E/q)-D)))

%% Part G

ca_sizes = [2*ca, 0.5*ca]; % Larger, Smaller

phi = acos(2*ca_sizes-1)

cl_beta = 2*(pi-phi+sin(phi))
```

```
A = int(c*cl_beta*y, y, y1, y2);

B = int((c^2)*(ec*cl_beta+cm_beta)*f, y, y1, y2);

rolling_power_sizes = V*(((A*(E/q)-D)+B*C)/(C*G+F*((E/q)-D)))
```